Sex-dependent role of hypocretin/orexin neurons in social behavior

Author Names and Affiliations:

Matthew Dawson[1,5,6], Dylan J Terstege[3,4,5], Naila Jamani[1,5,6], Dmitrii Pavlov[1,5,6], Mio Tsutsui[1,5,6], Raluca Bugescu[7], Jonathan R Epp[3,4,5], Gina M Leinninger[7], Derya Sargin[1,2,5,6]

Department of Psychology[1], Department of Physiology & Pharmacology[2], Department of Cell Biology and Anatomy[3], Cumming School of Medicine[4], Hotchkiss Brain Institute[5], Alberta Children's Hospital Research Institute[6], University of Calgary, Canada

Department of Physiology[7], Michigan State University, United States

Corresponding author:

Derya Sargin

Address:

University of Calgary

2500 University Ave Dr NW T2N 1N4

Calgary, AB, Canada

Phone: 403-2204349

Email: derya.sargin@ucalgary.ca

Abstract

Intraspecies social interactions are integral for survival and maintenance of society among all mammalian species. Yet, our understanding of the neural systems and mechanisms involved in the establishment of social connectedness are limited. Since their initial discovery as regulators of sleep/wakefulness and appetite in the brain, the hypocretin/orexin neurons have also been shown to play an essential role in modulating energy homeostasis, motivated and emotional behavior. These neurons are located exclusively in the hypothalamus which, regulates complex and goal-directed behaviors. The hypothalamus also plays an important role in the modulation of social behavior by encoding internal states. However, our understanding of the role of hypocretin neurons in social behavior is currently limited. To address this knowledge gap, we infused AAV encoding GCaMP6s into the lateral hypothalamus of female and male *Hcrt*$^{IRES\text{-}Cre}$ mice and performed fiber photometry to record the activity of hypocretin neuron population during social interaction. We then applied optogenetic inhibition of hypocretin neurons to determine the necessity of these neurons for social behavior. Our results indicate that hypocretin neurons exhibit a robust increase in activity in response to social interaction in both female and male mice. We demonstrate the hypocretin neuron population is differentially activated during interaction between familiar and stranger conspecifics. The optogenetic inhibition of hypocretin neuron activity during social behavior leads to a reduction in the amount of time mice are engaged in social interaction in males but not in females. Together, these data implicate the lateral hypothalamus hypocretin neurons as a key regulator within the larger network of neural systems involved in social behavior.

Introduction

Social behaviors are an essential component of survival for most organisms. Effectively and appropriately communicating with members of one's species enables an individual to gain access to information about foraging opportunities, potential mates and detection of threats. Interactions between conspecifics also provide the foundation for social group hierarchies,

providing members with protection from predation, support from others within the group, and obtaining emotional rewards. The importance of these gains for the success of an organism has led to lasting evolutionary conservation of social behaviors, over time reinforcing the development of complex neural systems for the more sophisticated and refined methods of social interaction we see in mammals.

For organisms to interact socially, each must collect and process sensory signals from their counterparts and their environment, integrate this information with their internal state (e.g., memories of prior experiences, affective state, evaluation of risks and rewards), determine the appropriate behavioral response for the situation, then perform a sequence of corresponding motor patterns. These processes must function in concert simultaneously and rapidly to accommodate the highly dynamic and unpredictable process of social interaction (Chen and Hong, 2018). The resulting neural networks required to orchestrate this are vast, and we are still early in our understanding of which anatomical regions of the brain are involved and what their individual contribution to social behaviors is. Despite the challenge inherent to elucidating the underlying mechanisms of such complicated behaviors, many recent studies have made significant advances in our understanding of the neural substrates of social behaviors. Research in rodent models has demonstrated the involvement of numerous cortical and subcortical regions in production and direction of social behavior (Anderson, 2016; Clancy et al., 1984; Gunaydin et al., 2014; Hashikawa et al., 2016; Y. Hashikawa et al., 2017; Hofer, 1996; Hong et al., 2014; Keller et al., 2006; Kingsbury et al., 2019; Li et al., 2016; Marlin et al., 2015; Okuyama, 2018; Takahashi et al., 2014; Unger et al., 2015; Veening and Coolen, 2014; Wei et al., 2021). These regions have been found to form extensive functional circuits between each other and work to govern the array of parallel processes required during social interaction.

The various regions of the hypothalamus play a particularly important role in the modulation of social behavior by encoding internal states (Lo et al., 2019). The evolutionarily conserved hypothalamus (Xie and Dorsky, 2017) regulates critical survival functions by

processing sensory and neuroendocrine signals and producing internal states to promote the organism to adjust its behavior to maintain homeostasis (Saper and Lowell, 2014). Certain internal states including emotion, memories of past experiences, motivation, and arousal are critical mediators in social behaviors as they determine the appropriate behavioral expression in response to incoming sensory information (Anderson, 2016). The modulatory power of these internal states over the social behavior of an animal is immense, to the degree that identical sensory stimuli and environmental conditions can elicit completely different behavioral responses based on the animal's internal state (Chen and Hong, 2018). A shared underlying characteristic to all these internal states is that behavioral arousal is required to produce attention to socially relevant signals and motivation to investigate and interact with the conspecific from which they originate. This systemic arousal directed towards social stimuli is a process central to social behavior and closely overlaps with the functional role of the lateral hypothalamus (LH). Since their discovery (de Lecea et al., 1998; Sakurai et al., 1998), the LH hypocretin (hcrt)/ orexin neurons have been shown to govern arousal (Bourgin et al., 2000; Del Cid-Pellitero and Garzón, 2011; Hasegawa et al., 2017, 2014; Yang et al., 2019), attentional (Fadel and Burk, 2010; Fadel and Frederick-Duus, 2008), and motivational (España et al., 2011, 2010; Fadel and Deutch, 2002; Vittoz et al., 2008) states which all contribute to modulation of social behavior. Hcrt neurons extensively project to and modulate the activity of brain regions involved in social interaction (Bisetti et al., 2006; Lungwitz et al., 2012; Samson et al., 2002; Sterley et al., 2018), social reward (Fadel and Deutch, 2002; Gunaydin et al., 2014; Payet et al., 2021; Wang et al., 2005), and social memory (Yang et al., 2013). However, their direct role in social behavior has been less studied.

To reveal how hcrt neuron activity contribute to social behavior, we employed Cre-inducible viral targeting combined with fiber photometry and optogenetic tools in *Hcrt*$^{IRES\text{-}Cre}$ mice during conspecific social interactions. We identified that hcrt neurons exhibit a robust increase in activity in response to social interaction. We demonstrate that hcrt neuron activity is more pronounced during interaction between unfamiliar mice compared to that observed during familiar

interactions. In contrast, exposing mice to familiar or novel objects does not lead to a difference in the activity of hcrt neurons suggesting that differential activity is driven primarily by social interactions. Finally, acute optogenetic inhibition of orexin neuron activity during social behavior disrupted social interaction in male mice without an effect in females. Together, our data compelling evidence for the sex-dependent role for hcrt neurons in social behavior.

Results

The activity of the LH hcrt neuron population increases in response to social investigation. To monitor the activity of hcrt neuron population in response to social approach and investigation, we used fiber photometry while performing a 3-chamber sociability test (Moy et al., 2004). We infused a Cre-dependent adeno-associated virus (AAV) encoding the fluorescent sensor GCaMP6s into the LH of *Hcrt*$^{IRES\text{-}Cre}$ mice. We found that >90 % of virus-labeled cells co-expressed Hcrt, while 58 % Hcrt+ cells were transduced with the virus (**Figure 1A, B; Figure 1-figure supplement 1**), similar to the previously published *Hcrt-cre* knock-in lines (Giardino et al., 2018; Mitchell et al., 2020). An optical fiber was implanted above the LH to allow the delivery of excitation light and collection of GCaMP6s fluorescence from hcrt neurons specifically (**Figure 1A, B**). After 5 min baseline recording in the middle zone of the 3-chamber apparatus, mice were given access to freely explore the chamber containing a confined social target (age and sex-matched novel conspecific) in one chamber and an empty non-social zone in other chamber (**Figure 1C**). We first averaged the hcrt Ca^{2+} signals in response to the social interaction that occurred within 2 sec of the social zone entrance and compared this with the Ca^{2+} signals in mice during their interaction with the empty cup in the non-social zone. In female mice, the hcrt neuron activity increased during entrance into the social and non-social zones (t=0 sec) and during interaction in the sniffing zones however, the activity between social and non-social zones remained non-significant (two-way ANOVA; effect of time: $F(2, 24) = 8.15$, $p = 0.002$, effect of zone: $F(1, 24) = 3.25$, $p = 0.084$) (**Figure 1D, E**). The area under the curve of the averaged hcrt Ca^{2+} responses were similar whether the female mice entered the social zone or the non-social

zone (paired t-test; $p = 0.39$) (**Figure 1F**). In male mice, the hcrt Ca^{2+} response started to increase within 1 sec prior to and reached maximum levels right after entrance into the social zone (**Figure 1G**). The hcrt Ca^{2+} response in male mice was significantly larger during and after entrance into the social zone when compared with the non-social zone (two-way ANOVA; effect of time: $F(2, 24) = 12.86$, $p = 0.0002$, effect of zone: $F(1,24) = 11.2$, $p = 0.0027$) (**Figure 1H**). The area under the curve of the averaged hcrt Ca^{2+} responses was significantly larger when male mice entered the social zone rather than the non-social zone (*paired t-test; $p = 0.025$) (**Figure 1I**).

We next compared the difference in the activity of hcrt neuron population while the mice are actively sniffing the confined conspecific (social sniffing zone) or the empty cup (non-social sniffing zone) (**Figure 1J**). During interaction with the social target, both female and male mice showed significantly larger maximum hcrt Ca^{2+} response (two-way ANOVA; effect of zone: $F(1, 16) = 9.23$, $p = 0.0078$, effect of sex: $F(1, 16) = 2.12$, $p = 0.16$) when compared to the time they spent in the non-social sniffing zone (**Figure 1K**). The frequency of activity (peaks/sec) during interaction with the social target was significantly larger compared to the non-social interaction, with females having an overall greater frequency (two-way ANOVA; effect of zone: $F(1, 16) = 11.26$, $p = 0.004$, effect of sex: $F(1, 16) = 7.82$, $p = 0.013$) (**Figure 1L**). The area under the curve of the hcrt Ca^{2+} signal changes was significantly larger when male mice interacted with the social target compared to the interaction in the non-social sniffing zone. This difference was not significant in females (two-way ANOVA; zone X sex interaction: $F(1, 16) = 5.07$, $p = 0.039$; Tukey's multiple comparisons test: Social vs non-social sniffing zone; males $p = 0.0055$, females $p = 0.86$) (**Figure 1M**).

Taken together, our data show that the response of the hcrt neuron population is larger when mice are actively sniffing the social conspecific when compared with the non-social exploration of an empty cup. This response is more prominent in males when they enter the social zone and interact with the social target, compared to females. However, both females and males

show an overall higher hcrt activity during the time they spent actively interacting with the social target in the sniffing zone.

Differential activity in the LH hcrt neuron population in response to familiar and novel social interaction. While the 3-chamber sociability test allows exploration of social interaction within a controlled setting, it does not allow direct social interaction. To determine the changes in the activity of hcrt neuron population during reciprocal and active social interaction, we performed fiber photometry in the resident mice while they are socially interacting in their home cage. Accordingly, we performed 5 min baseline recordings after which the resident mouse is first introduced to a cage partner (familiar conspecific) and allowed to interact for 5 min. After removing the familiar conspecific from the cage followed by a 5 min additional baseline recording, the resident mouse was introduced to a novel age-, sex- and strain-matched conspecific (stranger) and allowed to interact for 5 min (**Figure 2A**). This order was selected due to the possibility that potentially aggressive encounters with the stranger mice would increase the stress levels and confound subsequent interaction with a familiar mouse. In addition, the behavior of the familiar mouse towards the experimental mouse could be influenced by the odor of a previous stranger. To rule out the possibility of habituation, we determined changes in the hcrt neuron activity during subsequent interactions. We did not detect a difference in the hcrt neuron activity in the resident mouse when a familiar or a stranger mouse was introduced twice in a row (**Figure 2-figure supplement 1**). In the home cage, social interaction was initiated exclusively by the resident mouse approaching the mouse introduced into the cage (Fam: 1.41 ± 0.23 sec, Stranger: 1.6 ± 0.55 sec after introduction). Social approach was defined as the time the resident mouse initiated movement toward the social target (Gunaydin et al., 2014). Averaging the hcrt Ca^{2+} signals over time in both female and male mice showed that the hcrt activity in resident mice started to increase prior to initial approach, reached maximum levels right after the initial approach and sniffing and returned to baseline minutes after the first interaction (**Figure 2B, C**). The analysis of the area under the curve of the averaged hcrt Ca^{2+} traces showed that the hcrt Ca^{2+} response was

significantly larger in female and male resident mice during interaction with the unfamiliar conspecifics compared to the interaction with the familiar cage mates (two-way ANOVA; effect of conspecific: $F(1, 26) = 8.96$, $p = 0.006$, effect of sex: $F(1, 26) = 1.78$, $p = 0.19$) (**Figure 2D, E**). The maximum hcrt activity (max z-score ΔF/F) within 10 sec of initial approach was significantly greater during interaction between unfamiliar (resident and stranger) compared to that observed during familiar interactions in both female and male mice, with activity being larger during both types of social interaction in male mice compared with female mice (two-way ANOVA; effect of conspecific: $F(1, 26) = 8.01$, $p = 0.009$, effect of sex: $F(1, 26) = 8.29$, $p = 0.008$) (**Figure 2F**).

Next, we sought to determine the interaction between the initial large increase in hcrt activity with social behavior. We found a significant correlation between the first interaction-induced maximum hcrt activity and the time the resident mice spent sniffing the stranger mice (interaction %) within the subsequent 5 min of the social behavior task (Stranger: $r(13) = 0.58$, $^*p = 0.023$, Familiar: $r(13) = 0.37$, $p = 0.18$) **(Figure 2G)**. To further determine the relation between the hcrt signal and social behavior, we plotted the maximum hcrt activity (**Figure 2H**) along with the duration of the time spent by the resident mice sniffing the conspecifics (**Figure 2I**) over time. These data have been analyzed by three-way ANOVA with sex and conspecific as factors and time as a repeated measure. The maximum hcrt activity was the greatest during the first minute after mice met for the first time and declined over the subsequent minutes of the task (effect of time: $F(14, 364) = 21.26$, $p < 0.001$). This was found to be dependent on both sex (time X sex interaction: $F(14, 364) = 2.19$, $p = 0.007$; Tukey's multiple comparisons test: Male vs female at 20 sec $p = 0.013$, 40 sec $p = 0.033$, all other time points *p's* > 0.05), and conspecific (time X conspecific interaction: $F(14, 364) = 2.32$, $p = 0.004$; Tukey's multiple comparisons test: Stranger vs familiar at 20 sec $p = 0.035$, 40 sec $p = 0.009$, all other time points *p's* > 0.05) (**Figure 2H, I**) suggesting the engagement of this neuron population during initial contact. The time spent sniffing was significantly greater in males than females (effect of sex: $F(1, 26) = 4.62$, $p = 0.041$). Both female and male mice spent a significantly greater time sniffing the stranger mice compared with

familiar cage mates (effect of conspecific: $F(1, 26) = 11.81$, $p = 0.002$). Similar to the decrease in the hcrt activity, the initial difference in the time spent sniffing the stranger and familiar mice declined over time (time X conspecific interaction: $F(14, 364) = 3.46$, $p < 0.001$, Tukey's multiple comparisons test: Stranger vs familiar at 40 sec $p < 0.001$, 60 sec $p = 0.0013$, 80 sec $p = 0.005$ all other time points *p's* > 0.05).

Overall, these data show that hcrt neuron activity plays a significant and differential role in social interaction. We provide the first evidence that unfamiliar mice evoke a greater response in hcrt neuron activity than familiar mice. The peak hcrt signal induced by the initial approach and sniffing determines the subsequent time of interaction between the unfamiliar animals. Both female and male mice show an increase hcrt activity in response to stranger interaction compared with familiar however, male mice show greater hcrt activity and sniffing behavior regardless of the conspecific.

Differential hcrt neuron activity during social interaction persists in the novel cage but absent in response to object investigation. The choice of the home cage social interaction assay for our experiments allowed us to assess social interaction within the territorial environment of the resident mice. To determine whether the greater hcrt signal to a stranger conspecific persists in a non-territorial novel setting, we placed the experimental mice in a cage with novel bedding and performed fiber photometry during interaction with familiar and stranger mice (**Figure 3A**). In a novel cage, mice spent significantly more time engaging in non-social behaviors including rearing, ambulation and grooming compared to those in the home cage (**Figure 3-figure supplement 1A**). However, the time mice spent interacting with the familiar or the stranger conspecific was comparable in both cages (**Figure 3-figure supplement 1B-D**).

Similar to our observations in the home cage, the increase in the hcrt Ca^{2+} signal reached maximum levels in female and male mice right after the first approach and sniffing in the novel cage (**Figure 3B, C**). The quantification of the area under the curve of the averaged hcrt Ca^{2+} traces revealed a greater hcrt activity when mice interacted with a stranger compared to a familiar

mouse (two-way ANOVA; effect of conspecific: F(1, 18) = 4.91, p = 0.038) (**Figure 3D**). The maximum hcrt activity (max z-score ΔF/F) within 10 sec of initial approach was also significantly greater when mice interacted with a stranger compared with a familiar mouse (two-way ANOVA; effect of conspecific: F(1, 18) = 19.14, p = 0.0004). The hcrt activity was significantly larger in male mice during interaction with both familiar and stranger mice, when compared with females (two-way ANOVA; effect of sex: F(1, 18) = 4.87, p = 0.041) (**Figure 3E**), and was comparable to the signal observed during interaction in the home cage (**Figure 3-figure supplement 1E, F**). Similar to the home cage setting, the initial interaction-induced maximum hcrt activity correlated with the amount of interaction with the stranger conspecifics (**Figure 3F**). Altogether, these data show that the activity of hcrt neuron population is greater while mice are engaged with stranger conspecifics whether they are in their territorial home cage environment or in a novel cage, with higher hcrt activity and sniffing behavior in males in both settings.

To identify whether the differential activity in the hcrt neuron population is a general response to novelty or specific to social interaction, we performed fiber photometry while mice were exposed to a familiar or a novel object in their home cage. Experimental mice were pre-exposed to the familiar object for at least 3 days in their home cage (Okuyama et al., 2016). In this task, we presented the experimental mice with a familiar or a novel object following a 5 min baseline recording (**Figure 3G**). In both female and male mice, we observed an increase in the hcrt Ca^{2+} signal in response to initial approach and interaction with the objects (**Figure 3H**). In contrast to the differential hcrt signal observed during familiar and stranger mouse interactions, both the maximum hcrt Ca^{2+} signal and the area under the curve for the first 2 min of interaction were similar during novel and familiar object interactions (**Figure 3I, J**). This showed that the significant difference in the hcrt Ca^{2+} signal during social interaction was absent when mice interacted with the familiar or novel objects, suggesting that the differential activity is specific to social interaction.

Because female and male mice employ different strategies (Anderson, 2016; van den Berg et al., 2015), we further analyzed the two distinct modalities of social investigative behaviors that the experimental mice engaged in, including anogenital sniffing (examination of the anogenital area of the conspecific) and the head/torso sniffing (examination of the head and torso region of the conspecific (Lee et al., 2019; Sterley et al., 2018). Both female and male mice spent more time sniffing the anogenital and head/torso region of the stranger mice when compared with the familiar conspecifics, with males spending a greater time engaged in anogenital sniffing compared to females (Anogenital sniffing: two-way ANOVA; effect of conspecific: $F(1, 26) = 18$, $^{**}p = 0.002$, effect of sex: $F(1, 26) = 8.19$, $^{**}p = 0.0082$; Head/torso sniffing: two-way ANOVA; effect of conspecific: $F(1, 26) = 3.17$, $p = 0.087$, effect of sex: $F(1, 26) = 0.99$, $p = 0.33$) (**Figure 3-figure supplement 2A, B**). The analysis of the hcrt activity peaks time locked to each behavior yielded a significantly larger signal in female and male mice while they were engaged in the anogenital and head/torso sniffing of the stranger mice, compared to sniffing the familiar conspecifics (Anogenital sniffing: two-way ANOVA; effect of conspecific: $F(1, 26) = 6.16$, $^{*}p = 0.02$, effect of sex: $F(1, 26) = 3.62$, $p = 0.068$; Head/torso sniffing: two-way ANOVA; effect of conspecific: $F(1, 26) = 7.21$, $^{*}p = 0.012$, effect of sex: $F(1, 26) = 2.6$, $p = 0.12$) (**Figure 3-figure supplement 2C-F**). These data showed a stronger anogenital sniffing drive and a borderline increase in the activity of the hcrt neuron population during anogenital sniffing in male mice compared to females.

Taken together, our data showed that the activity of the LH hcrt neuron population increases in response to social or object investigation. However, while the larger hcrt neuron activity in response to novel social interaction indicates social discrimination, this difference in activity is absent when mice interact with familiar or novel objects. The sex differences with males responding to social interaction with larger anogenital sniffing and greater hcrt Ca^{2+} response compared with females are also absent when mice are interacting with objects.

Inhibition of hcrt neuron activity disrupts social behavior in male mice. Having established that the activity of hcrt neuron population is highly responsive to social interaction, we next investigated whether hcrt neurons are required for social behavior. We infused a Cre-dependent adeno-associated virus (AAV) encoding EYFP (controls) or the blue light-activated chloride channel (iC++) (Berndt et al., 2016) into the LH of *Hcrt*$^{IRES\text{-}Cre}$ mice (**Figure 4A, B, Figure 4-figure supplement 1**). Because the first social interaction yields the maximum signal, which correlates with the subsequent interaction amount, we employed a photoinhibition protocol by silencing hcrt neurons in resident mice prior to the introduction of familiar or stranger conspecifics into the home cage (**Figure 4C**). The social interaction test was repeated on two separate days and the order of the conspecific was counterbalanced across different days. Social interaction was quantified as the summation of anogenital and head/torso sniffing. In female mice, the optogenetic inhibition of hcrt activity did not affect the time spent interacting with familiar or stranger conspecifics (two-way ANOVA; effect of group: $F(1, 28) = 1.64$, $p = 0.21$, effect of conspecific: $F(1, 28) = 3.41$, $p = 0.07$) (**Figure 4D**). In contrast, male mice spent significantly less time interacting with conspecifics when hcrt activity was inhibited (two-way ANOVA; effect of group: $F(1, 24) = 13.82$, $p = 0.001$, effect of conspecific: $F(1, 24) = 2.66$, $p = 0.12$) (**Figure 4E**).

To determine whether sociability is affected similarly in a more controlled setting in which the stranger mouse is confined, we tested mice in a 3-chamber test while inhibiting hcrt neuron activity. While we detected no difference for sociability in females (two-way ANOVA; effect of group: $F(1, 28) = 2.59$, $p = 0.12$, effect of zone: $F(1, 28) = 26.56$, $p < 0.001$) (**Figure 4F, G**) and control males (**Figure 4F, H**), all showing a greater preference for the confined stranger, male iC++ mice spent comparable time in the social and non-social sniffing zones (two-way ANOVA; group X zone interaction: $F(1, 22) = 4.81$, $p = 0.039$; Tukey's multiple comparisons test: EYFP social vs non-social $p = 0.029$, iC++ social vs non-social $p = 0.99$) (**Figure 4H**).

Because hcrt neuron activity is linked to locomotion (Karnani et al., 2020) and can be regulated by stress (Grafe et al., 2018, 2017; Sargin, 2019), we next investigated whether

inhibition of hcrt neurons affects locomotor or anxiety-like behavior. We performed open field and elevated plus maze tests in the presence of blue light in EYFP- and iC++ expressing female and male mice. Acute inhibition of hcrt neuron activity during open field test did not lead to changes in distance traveled (two-way ANOVA; effect of group: $F(1, 25) = 1.46$, $p = 0.24$), or the time spent in the outer or the inner zone of the open field apparatus (two-way ANOVA; effect of group for time in outer zone: $F(1, 25) = 1.45$, $p = 0.24$, effect of group for time in inner zone: $F(1, 25) = 1.45$, $p = 0.24$) in iC++ female and male mice, compared with mice expressing EYFP (**Figure 4-figure supplement 2A-D**). In the open field test, both groups of female mice traveled a greater distance than male mice, indicating greater locomotor activity in females regardless of group (two-way ANOVA; effect of sex: $F(1, 25) = 4.62$, $^*p = 0.042$). Female mice also spent more time in the outer zone (two-way ANOVA; effect of sex: $F(1, 25) = 4.64$, $^*p = 0.041$) and less time in the inner zone of the open field (two-way ANOVA; effect of sex: $F(1, 25) = 4.64$, $^*p = 0.041$), compared with male mice (**Figure 4-figure supplement 2A-D**). In the elevated plus maze, we did not detect a difference in locomotion (two-way ANOVA; effect of group: $F(1, 23) = 0.64$, $p = 0.43$, effect of sex: $F(1, 23) = 3.02$, $p = 0.09$) or anxiety-like behavior between the groups (two-way ANOVA; effect of group for time in closed arms: $F(1, 23) = 1.21$, $p = 0.28$, effect of group for time in open arms: $F(1, 23) = 1.19$, $p = 0.28$) or sexes (two-way ANOVA; effect of sex for time in closed arms: $F(1, 23) = 1.07$, $p = 0.31$, effect of sex for time in open arms: $F(1, 23) = 0.67$, $p = 0.42$) (**Figure 4-figure supplement 2E-H**).

Overall, acute optogenetic inhibition of hcrt neuron activity significantly reduced the time resident male mice spent interacting with the conspecifics, and decreased the preference of male mice for the social conspecific without affecting locomotor activity or anxiety-like behavior. In females, acute inhibition of hcrt neuron activity did not affect social interaction. These data suggest that hcrt neurons are necessary for normative social behavior in male mice while in females, the potential recruitment of different neural circuits may overcome the effects of reduced hcrt activity on social interaction.

Discussion

Discrete neural subpopulations in the hypothalamus play a critical role in producing and modulating a variety of social behaviors, such as mating, aggression, and social bonding (Hashikawa et al., 2016; K. Hashikawa et al., 2017; Y. Hashikawa et al., 2017; Hull and Dominguez, 2007; Scott et al., 2015; Wu et al., 2014; Yoshihara et al., 2018). Similarly, research into the functional roles of hcrt neurons has begun to suggest that these cells are involved in the neural substrates of social processes, but the nature and extent of their involvement has not yet been determined. Here, using a combination of fiber photometry, optogenetic inhibition and social interaction assays, we characterized the role of hcrt neuron activity in social behavior. We demonstrate for the first time that the activity of hcrt neuron population is regulated by social approach and interaction and is critical for social behavior in a sex-dependent manner.

Photometry recordings revealed that hcrt neurons in female and male mice exhibit a robust increase in activity in response to social interaction. The elevation in activity was prominent during indirect social contact in the 3-chamber social interaction test or during reciprocal social interaction in the familiar home cage or less familiar novel cage. Moreover, hcrt neuron activity was more pronounced during interaction between unfamiliar mice compared to the increased activity observed during familiar interactions. These experiments provide the first evidence that the discrimination between familiar and unfamiliar conspecifics is differentially encoded by the hcrt neuron activity. In contrast, the increase in hcrt neuron activity remained the same when mice interacted with familiar or novel objects, suggesting that a greater population of hcrt neurons is being recruited in response to social novelty.

Earlier work has implicated that hcrt signaling plays a role in social behavior. Accordingly, male *Hcrt receptor 1* gene (*Hcrtr1*$^{-/-}$) null mutant mice exhibit reduced sociability and decreased preference for social novelty compared to wild type mice (Abbas et al., 2015). Male orexin null mutant mice show diminished behavioral response to an intruder in a resident-intruder paradigm (Kayaba et al., 2003). A microdialysis study in human epileptic patients found maximal hcrt

release during social interactions (Blouin et al., 2013). While orexin/ataxin-3- transgenic mice with hcrt cell loss show deficits in social memory (Yang et al., 2013). Supported by these studies, our data suggest a novel role for hcrt neuron activity states in the encoding of social discrimination. We also report a significant correlation between initial social approach and interaction-induced hcrt neuron activity and the subsequent time mice spent engaging with stranger conspecifics, suggesting that the initial approach-induced engagement of the hcrt neurons determines how long the stranger mice will interact with each other within the next minutes of the test.

While both females and males show greater hcrt activity in response to social interaction, we obtained sex differences in the extent of hcrt activity and social interaction in females compared with males. Overall, both the hcrt Ca2+ signal and amount of time spent in social sniffing habituated faster in females throughout the course of a 5 min reciprocal social interaction test. A difference in sex-dependent neural and social engagement is not surprising given the variable strategies utilized by female and male mice in social behavior (Okuyama et al., 2016; Rao et al., 2019). Yet, while the optogenetic inhibition of hcrt neurons resulted in a deficit in the normal behavior of male mice towards conspecifics, this did not lead to a change in sociability of females. This difference in the activity phenotype of hcrt neurons may represent sex-specific differences in local LH hcrt neuron network dynamics, which aligns with the previously discussed sex differences seen in other hypothalamic cell subpopulations (K. Hashikawa et al., 2017). Whether the recruitment of different populations of hcrt projection neurons play a role in sex-dependent differences will provide significant insight into sex differences in social behavior and may have important implications for disorders associated with social deficits and that are more prevalent in men compared with women (Silber et al., 2002; Werling and Geschwind, 2014).

Hcrt neurons are key regulators of sleep, wakefulness and arousal (Carter et al., 2012; de Lecea, 2021; Inutsuka and Yamanaka, 2013; Sakurai, 2005; Tyree et al., 2018). Increased hcrt activity reduces sleep to wake transitions (Adamantidis et al., 2007; Carter et al., 2009) while reduced hcrt signaling or ablation of hcrt neurons has been associated with deficits in wakefulness

and narcolepsy, respectively (Hara et al., 2001; Peyron et al., 2000; Sasaki et al., 2011; Tsunematsu et al., 2011). Decreased arousal and wakefulness may contribute to a reduced interest for social interaction. However, we did not find a change in locomotor activity upon acute hcrt neuron inhibition, suggesting that reduced interaction with conspecifics is not simply due to sedation. Given the strong association of narcolepsy and social impairments (Morse and Sanjeev, 2018; Quaedackers et al., 2019), a correlation between potential changes in sleep/wakefulness parameters and social interaction upon acute hcrt inhibition will provide more insight. Due to the involvement of hcrt in stress response (Grafe et al., 2018, 2017; Sargin, 2019), manipulation of hcrt neuron activity may interfere with generalized anxiety states. However, we did not observe changes in general anxiety-like behavior with acute hypocretin inhibition, suggesting that the association between reduced hcrt activity and social interaction may not be attributed solely to changes in anxiety levels.

Overall, our findings provide a thorough characterization of hcrt neuron activity in social interaction, and situate the hcrt system as a critical part of a larger network that plays an integral role in the modulation of social behavior. The observed sex differences further emphasize the need for the incorporation of sex as a biological variable in the design of studies focusing on the modulation of social behavior to understand the underlying mechanisms and circuits. Insights into the role of the hcrt system in social behavior will particularly be important in paving the way for novel treatment strategies targeting neuropsychiatric disorders associated with social deficits.

Materials and Methods

Animals

We used female and male mice (10- to 16-week old) *Hcrt*$^{IRES\text{-}Cre}$ mice on a C57BL6/J background. Age-, and sex-matched C57BL6/J mice were used as strangers. Mice were housed in standard housing conditions on 12 h light/dark cycle (light on at 07:00) with water and food available *ad libitum*. All experiments were conducted at the same time each day (12:00 – 16:00

pm). All experimental procedures were performed in accordance with the guidelines established by the Canadian Council on Animal Care and were approved by the Life and Environmental Sciences Animal Care Committee at the University of Calgary.

Generation of the *Hcrt*$^{IRES\text{-}Cre}$ knock-in mouse line

Hcrt$^{IRES\text{-}Cre}$ mice were generated and gifted by Dr. Gina Leinninger. Briefly, a targeting vector for homologous recombination was generated by inserting an internal ribosome entry site (IRES)-Cre cassette into the 3' end of the *hypocretin* mRNA product. A frt-flanked neo cassette was placed upstream of the IRES-Cre sequence. This *Hcrt*$^{IRES\text{-}Cre}$ targeting vector was linearized and electroporated into C57/Bl6 mouse embryonic stem cells. DNA from ES cell clones was analyzed via qPCR for loss of homozygosity using Taqman primer and probes for the genomic *Hcrt* insertion sites (*Hcrt:* Forward: TTTACCAAGAGACTGACAGCG, Reverse: CGGAGTCTGAACCCATCTTC, Probe: TCCTTGTCCTGATCCAAACTTCCCC). *NGF* was used as a copy number control (Soliman et al., 2007). Putative positive ES clones were expanded, confirmed for homologous recombination by Southern blot for neo and injected into blastocysts to generate chimeric mice. Male chimeras were bred with C57BL/6 albino females and produced germline progeny that express *Cre* and/or wild type *hcrt* (as assessed via PCR genotyping), confirming successful establishment of the *Hcrt*$^{IRES\text{-}Cre}$ line. (Forward Cre: CAC TGA TTT CGA CCA GGT TC, Reverse Cre: CAT CGC TCG ACC AGT TTA GT; Forward Hcrt wt: CTG GCT GTG TGG AGT GAA A, Reverse Hcrt wt: GGG GGA AGT TTG GAT CAG G. Cre band = 255 bp, Hcrt wt band = 460 bp).

Hcrt$^{IRES\text{-}Cre}$ mice were initially bred with *FlpO-Deleter* mice (Jackson Laboratories *B6.129S4-Gt(ROSA)26Sor*$^{tm2(Flp^{*})Sor}$*/J*, stock #012930) to remove the frt-flanked neo cassette. Neo-deleted *Hcrt*$^{IRES\text{-}Cre}$ mice were then bred with C57/BL/6J mice (Jackson Laboratory, Strain #000664) to propagate the line.

Stereotaxic Virus Injection and Optical Fiber Implantation

Mice were anaesthetized with 5% isoflurane before being transferred to a stereotaxic head frame (Kopf Instruments) and maintained at 2% isoflurane. Mice received analgesia (5 mg/kg meloxicam, s.c.) and fluid support (Lactated Ringer's solution, s.c.) during surgery. Viral infusion was performed using a glass micropipette attached to a Nanoject III infusion system (Drummond Scientific) at 25 nl/sec for 10 sec. The infusion pipette was kept in place for 5 min after viral delivery and slowly elevated over 5 min. The following coordinates were used for virus injections: LH (from Bregma: AP -1.5 mm; ML ±1.0 mm; DV -5.2 mm). For fiber photometry experiments, mice received a unilateral infusion of AAV9-CAG-flex-GcAMP6s.WIRE.SV40 (Addgene viral prep # 100842-AAV9; 1.5 x 10^{13} vg/ml, 250 nl). For optogenetic experiments, mice received bilateral infusions of AAV2/9-EF1a-DIO-iC++-EYFP (Canadian Neurophotonics Platform Viral Core Facility RRID:SCR_016477; 1.7 x 10^{13} vg/ml, 250 nl per hemisphere) or AAV2/9-EF1a-DIO-EYFP (Canadian Neurophotonics Platform Viral Core Facility RRID:SCR_016477; 1.9 x 10^{13} vg/ml, 250 nl per hemisphere).

For fiber photometry experiments, viral infusions were followed by implantation of mono fiber optic cannulae (Neurophotometrics; 400 um, AP -1.5 mm; ML ±1.0 mm; DV -5.2 mm). For optogenetic experiments, dual fiber optic cannulae (Doric Lenses; 200 um, AP -1.5 mm; ML ±1.0 mm; DV -4.9 mm) were used. Implants were secured to the skull using super glue and dental cement. Behavior experiments were performed at least 3 weeks after surgery.

***In vivo* Fiber Photometry Recording and Analysis**

A Doric Lenses fiber photometry system with an LED driver and console was used to deliver the 405 nm isosbestic control and 465 nm excitation light during recordings. LEDs were connected to a Mini Cube filter set and a dichroic mirror array was used to permit simultaneous delivery of excitation light through a low autofluorescence mono fiber-optic patch cord to the fiber optic cannulae. The signal was detected by a photoreceiver (Newport Visible Femtowatt Photoreceiver Module Model 2151). A lock-in amplification mode controlled by the Doric Studio software was implemented (modulation frequencies: 208.6 Hz for 456 nm, 166.9 Hz for 405 nm,

cut-off frequency for demodulated signal: 12 Hz). Light power was calibrated to deliver 30 μW light at the tip of the fiber using a photometer (Thor Labs).

The Doric Lenses fiber photometry console was set to trigger recording on remote delivery of a time-to-live (TTL) pulse from a separate computer running ANY-maze behavior capture software to time lock video and photometry recordings. Data from photometry and behavioral recordings were extracted and exported to MATLAB (MathWorks). Using custom MATLAB analyses, the 405 nm channel was used as an isosbestic control and the data recorded using this channel was fit to a biexponential decay. Data from the Ca^{2+}-dependent 465 nm channel were then linearly scaled using the fitted decay of the isosbestic channel, correcting for any photobleaching which occurred during the recordings (Meng et al., 2018). The resulting vector was converted to a ΔF/F trace as previously described (Evans et al., 2022), and each trace was normalized as a z-score (Reichenbach et al., 2022). Z-scored ΔF/F traces were analyzed for area under the curve, peak frequency, and maximum fluorescence.

Area under the curve was operationally defined as the summed area between the X-axis and the z-scored ΔF/F trace. Comparisons of AUC during specific behaviours were normalized by the summed duration of the behavioural epochs of interest. Peak frequency was refined using a peak detection filter of 2 standard deviations above the median z-scored ΔF/F value of the recording session (Evans et al., 2022; Moda-Sava et al., 2019). For all behaviour-specific analyses, photometry and behavioural timeseries vectors were aligned using nearest-neighbours approximation to account for differences in framerates across recording modalities.

***In vivo* Optogenetic Inhibition**

Mice expressing EYFP (AAV2/9-EF1a-DIO-EYFP) or the inhibitory opsin iC++ (AAV2/9-EF1a-DIO-iC++-EYFP) were used for optogenetic inhibition experiments. Laser driver (Opto Engine LLC) was connected to a 1 x 2 fiber optic rotary joint (Doric Lenses) attached to a dual fiber-optic patch cord. Mice were habituated to the patch cord for 5 min prior to starting the

behavior experiments. Blue light (470 nm, 17 mW) was delivered continuously via ANY-Maze software-controlled AMi-2 optogenetic interface (Stoelting Co.) connected to the laser driver.

Behavioral Testing

The order of behavior tests was counterbalanced to control for any effect of testing order. Before each test, the area around and under cages or the surfaces of the apparatus were sprayed with 70% ethanol and wiped down with paper towel to reduce any residual odour. Prior to testing, mice were handled and habituated to the fiber optic patch cord for 4 days.

3-Chamber Social Interaction Test

The 3-chamber social interaction test was performed in two-stages in an acrylic 105 cm X 45 cm apparatus containing two plexiglass dividers, splitting the chamber into three equal areas. During the habituation stage, each mouse was first placed in the middle chamber for 5 min. The removal of the dividers allowed mice to freely explore the chamber for an additional 5 min. During the test stage, one area contained a sex- and age-matched C57BL/6J mouse confined in an inverted pencil cup (social zone) while the other area contained an empty cup (non-social zone). Mice were first placed in the middle chamber with dividers in place for 5 min. Dividers were then removed and mice were allowed to explore the chamber for 5 min. Time spent in each area was tracked and analyzed using ANY-Maze video tracking software (Stoelting Co.).

Reciprocal Social Interaction Test

To examine reciprocal social behavior, resident experimental mice were kept in their home cage. Cage mates were separated for at least 15 min. For fiber photometry experiments, 5 min after being connected to the fiber optic patch cord, the cage mate (familiar mouse) of the experimental mouse was placed in the home cage and animals were allowed to freely interact for 5 min. 5 min after removal of the cage mate, a sex- and age-matched C57BL/6J mouse (stranger mouse) was placed in the home cage, and mice were allowed to freely interact for 5 min. For optogenetic experiments, the tests were spread across two consecutive days to reduce the likelihood of

potential effects of prolonged light delivery and continual photoinhibition. The order of familiar or stranger mice introduced into the home cage of the experimental mice was counterbalanced across days. Blue light (470 nm, 17 mW) was turned on to allow 2 min of initial inhibition before the introduction of the familiar or stranger mouse. The experimental mouse and conspecific were allowed to freely interact for 5 min during continuous light delivery. Reciprocal social behavior in a novel cage was examined using the similar paradigm above in a novel mouse cage with new bedding material. All videos were recorded using ANY-Maze video tracking software (Stoelting Co.).

Social Behavior Analysis

We used the open-source automated positional tracking and behavioral classifications algorithms DeepLabCut (DLC; (Lauer et al., 2021) and Simple Behavior Analysis (SimBA; (Nilsson et al., 2020) to allow for unbiased, high-precision quantification and machine analysis of social behavior. A subset of social interaction trials was also manually scored by an experimenter blind to the groups to validate the resulting behavioral classifiers. Behavioral classifiers from SimBA quantified social behavior as the time the experimental mice engage in head-torso sniffing (snout of the experimental mouse was in direct proximity or direct contact with the head or torso of a conspecific) and anogenital sniffing (snout of the experimental mouse was in direct proximity to the anogenital region of a conspecific, including when actively following behind and sniffing a conspecific).

Machine Scoring

For automated analysis of social behavior using behavioral classification algorithms, video recordings of social behavior experiments were first exported from ANY-maze to 20 frames-per-second MP4 video files. A subset of these video files was imported into DLC, where the experimenter blinded to the groups labelled the nose, left & right ears, left & right latissimus dorsi, tail base, and the centre of the torso for each animal present in the frames. These frames were

then used by DLC to train the neural network to label the seven body parts described above. The trained neural network then analyzed all video recordings of social behavior experiments to track and plot the Cartesian coordinates of animals' body parts for every frame of each video. This effectively provided the detailed spatial location of mice for every point in time throughout the experiment.

The results of the positional tracking analysis from DLC were exported to SimBA. We used a supervised-learning deep neural network within SimBA to create predictive classifiers for head-torso and anogenital sniffing. The resulting predictive classifiers were then used to automatically identify patterns in the positional data from DLC. Automated behavioral labels were validated for accuracy by reviewing visualizations of classification results produced by SimBA.

For verification, all results from SimBA were visualized and reviewed by the experimenter, and a subset of experiments were hand-scored to compare against the results of the automated analysis. The results of SimBA's predictive classification for each experiment were exported for both analysis of behavior alone and combined analysis with the photometry recordings from the respective experiment. For photometry experiments, SimBA data and raw photometry traces were imported and aligned by a custom MATLAB script. For optogenetic experiments, SimBA data were analyzed and plotted.

Object Interaction Test

Mice were made familiar with an object (a small plastic puzzle piece) placed in their home cage for 72 h prior to the day of testing. A round glass marble was used as a novel object. 5 min after being connected to the fiber optic patch cord, novel or familiar object was introduced into the home cage of the experimental mouse. Each mouse was allowed to interact with the objects for 5 min. Videos were tracked and the time spent with each object was analyzed using ANY-Maze software (Stoelting Co.).

Open Field Test

Mice were placed in an acrylic 40 cm x 40 cm apparatus and allowed to explore for 5 min. Blue light (470 nm, 17 mW) was kept on continuously while the animal was in the open field. Videos were recorded and the total distance traveled, and the time spent in the outer and inner zones were analyzed using ANY-Maze video tracking software (Stoelting Co.).

Elevated Plus Maze

Mice were placed in the center of a plus-shaped apparatus consisting of two closed (36 cm) and two open (36 cm) arms. Blue light (470 nm, 17 mW) was kept on continuously while mice were allowed to explore for 5 min. Videos were recorded and the total distance traveled, and the time spent in each arm were analyzed using ANY-Maze video tracking software (Stoelting Co.).

Slice Electrophysiology

400 µm coronal slices comprising the LH were obtained in ice-cold oxygenated sucrose-substituted artificial cerebrospinal fluid (ACSF) using a Leica VT1000 S vibratome. Slices were recovered in aCSF (128 mM NaCl, 10 mM D-glucose, 26 mM $NaHCO_3$, 2 mM $CaCl_2$, 2 mM $MgSO_4$, 3 mM KCl, 1.25 mM NaH_2PO_4, pH 7.4) for a minimum of 2 hours. During recovery and recordings, slices were saturated with 95% O_2/5% CO_2 at 30°C. Recording was performed in oxygenated aCSF flowing at a rate of 3-4 ml/min. The internal patch solution contained 120 mM potassium gluconate, 10 mM HEPES, 5 mM KCl, 2 mM $MgCl_2$, 4 mM K_2-ATP, 0.4 mM Na_2-GTP, 10 mM Na_2-phosphocreatine, with pH adjusted to 7.3. Neurons were visualized using IR-DIC on an Olympus BX51WI microscope and hcrt neurons were identified based on the expression of EYFP. Whole-cell recordings were obtained in current clamp mode using a MultiClamp 700B amplifier (Molecular Devices). Optogenetic inhibition through activation of iC++ was elicited using CoolLED pE-300^{ultra} illumination system at 470 nm. Data were filtered at 4 kHz and digitized at 20 kHz using Digidata 1550B and Clampex software (Molecular Devices).

Histology, Immunohistochemistry and Imaging

Mice were then deeply anaesthetized by isoflurane and transcardially perfused with 0.1 M PBS and 4% paraformaldehyde (PFA). Brains were extracted and post-fixed in 4 % PFA for 24 h

and cryoprotected in 30% sucrose in 0.1 M PBS for 3-5 days until sunk. Brains were frozen and 40 μM thick coronal sections were obtained using a cryo-microtome (ThermoFisher) and collected in 6 series. Sections were stored in an antifreeze solution containing 30 % ethylene glycol, and 20 % glycerol in 0.1 M PBS and stored at -20°C for further analysis.

For immunolabeling, sections were washed three times in 0.1 M PBS for 10 min each. Sections were incubated with goat anti-hypocretin-1/orexin A antibody (1:500, Santa Cruz, sc-8070) and/or rabbit anti-melanin concentrating hormone (MCH) (1:500, Phoenix Pharmaceuticals) diluted in 3 % normal donkey serum, 0.3 % Triton-X and 0.1 M PBS for 24 h. After three washes with 0.1 M PBS for 10 min each, sections were incubated with donkey anti-goat Alexa Fluor 594 (1:500, Jackson ImmunoResearch) and/or anti-goat Alexa Fluor 647 (1:500, Invitrogen) diluted in 0.1 M PBS for 24 h. After three 10 min washes with 0.1 M PBS, sections were mounted on glass slides and coverslipped with PVA-DABCO mounting medium.

Sections were imaged using an Olympus FV3000 confocal microscope. Images were acquired with a 10X and 60X oil immersion objectives, with the aperture set to 1 Airy unit. Z-stack image sequences were maximum intensity projected as a 2D image using Fiji. 2-3 sections comprising the LH were analyzed per mouse. Quantification of cells labeled with GFP and hypocretin-1 was performed using Fiji image processing software. Only mice with accurate stereotaxic targeting and viral expression were included in the analyses.

Statistical Analysis

Statistical analysis was performed using GraphPad Prism 9, except three-way ANOVAs which were conducted using Statistica software. Tukey's multiple comparisons tests were applied when appropriate. All statistical data are reported in Supplemental Table.

Acknowledgements

We thank the transgenic cores at University of Michigan and Van Andel Research Institute for assistance generating *Hcrt*$^{IRES\text{-}Cre}$ mice. David P. Olson graciously shared the Cre-inducible Rosa$^{eGFP\text{-}L10a}$ reporter line used in these studies. Funding for this study was provided by an

NSERC Discovery Grant (RGPIN-2020-05305) and a Brain Canada and Azrieli Foundation Future Leader in Canadian Brain Research grant to DS, an NSERC Discovery Grant (RGPIN-2018-05135) to JRE. DJT received fellowships from NSERC and the Canadian Open Neuroscience Platform. DP received Harley Hotchkiss-Samuel Weiss Postdoctoral Fellowship.

Author contributions

D.S. and M.D. designed the experiments and wrote the manuscript. R.B. and G.M.L. designed and made the mouse line. N.J. and M.T. performed the surgeries. M.D. and D.P. performed the behavioral experiments. M.D. performed the histological procedures. D.S., M.D., D.J.T. and J.R.E. conducted the analysis.

Data availability

All data that support the findings of this study are present in the manuscript and the supplementary materials, and are available from the corresponding author upon request.

Code availability

All custom scripts used for photometry analysis are publicly available in a GitHub repository (https://github.com/dterstege/PublicationRepo/tree/main/Dawson2022).

Declaration of Interests

The authors declare no competing interests.

References

Abbas MG, Shoji H, Soya S, Hondo M, Miyakawa T, Sakurai T. 2015. Comprehensive Behavioral Analysis of Male Ox1r−/− Mice Showed Implication of Orexin Receptor-1 in Mood, Anxiety, and Social Behavior. *Front Behav Neurosci* **9**. doi:10.3389/fnbeh.2015.00324

Adamantidis AR, Zhang F, Aravanis AM, Deisseroth K, de Lecea L. 2007. Neural substrates of awakening probed with optogenetic control of hypocretin neurons. *Nature* **450**:420–424. doi:10.1038/nature06310

Anderson DJ. 2016. Circuit modules linking internal states and social behaviour in flies and mice. *Nat Rev Neurosci* **17**:692–704. doi:10.1038/nrn.2016.125

Berndt A, Lee SY, Wietek J, Ramakrishnan C, Steinberg EE, Rashid AJ, Kim H, Park S, Santoro A, Frankland PW, Iyer SM, Pak S, Ährlund-Richter S, Delp SL, Malenka RC, Josselyn SA, Carlén M, Hegemann P, Deisseroth K. 2016. Structural foundations of optogenetics: Determinants of channelrhodopsin ion selectivity. *Proc Natl Acad Sci U S A* **113**:822–829. doi:10.1073/pnas.1523341113

Bisetti A, Cvetkovic V, Serafin M, Bayer L, Machard D, Jones BE, Mühlethaler M. 2006. Excitatory action of hypocretin/orexin on neurons of the central medial amygdala. *Neuroscience* **142**:999–1004. doi:10.1016/j.neuroscience.2006.07.018

Blouin AM, Fried I, Wilson CL, Staba RJ, Behnke EJ, Lam HA, Maidment NT, Karlsson KÆ, Lapierre JL, Siegel JM. 2013. Human hypocretin and melanin-concentrating hormone levels are linked to emotion and social interaction. *Nat Commun* **4**:1547. doi:10.1038/ncomms2461

Bourgin P, Huitrón-Résendiz S, Spier AD, Fabre V, Morte B, Criado JR, Sutcliffe JG, Henriksen SJ, de Lecea L. 2000. Hypocretin-1 modulates rapid eye movement sleep through activation of locus coeruleus neurons. *J Neurosci* **20**:7760–7765. doi:10.1523/JNEUROSCI.20-20-07760.2000

Carter ME, Adamantidis A, Ohtsu H, Deisseroth K, de Lecea L. 2009. Sleep homeostasis modulates hypocretin-mediated sleep-to-wake transitions. *J Neurosci* **29**:10939–10949. doi:10.1523/JNEUROSCI.1205-09.2009

Carter ME, Brill J, Bonnavion P, Huguenard JR, Huerta R, de Lecea L. 2012. Mechanism for Hypocretin-mediated sleep-to-wake transitions. *Proc Natl Acad Sci U S A* **109**:E2635-44. doi:10.1073/pnas.1202526109

Chen P, Hong W. 2018. Neural Circuit Mechanisms of Social Behavior. *Neuron* **98**:16–30. doi:10.1016/j.neuron.2018.02.026

Clancy AN, Coquelin A, Macrides F, Gorski RA, Noble EP. 1984. Sexual behavior and aggression in male mice: involvement of the vomeronasal system. *J Neurosci* **4**:2222–2229. doi:10.1523/JNEUROSCI.04-09-02222.1984

de Lecea L. 2021. Twenty-Three Years of Hypocretins: The 'Rosetta Stone' of Sleep/Arousal Circuits. *Front Neurol Neurosci* **45**:1–10. doi:10.1159/000514961

de Lecea L, Kilduff TS, Peyron C, Gao X, Foye PE, Danielson PE, Fukuhara C, Battenberg EL, Gautvik VT, Bartlett FS 2nd, Frankel WN, van den Pol AN, Bloom FE, Gautvik KM, Sutcliffe JG. 1998. The hypocretins: hypothalamus-specific peptides with neuroexcitatory activity. *Proc Natl Acad Sci U S A* **95**:322–327. doi:10.1073/pnas.95.1.322

Del Cid-Pellitero E, Garzón M. 2011. Hypocretin1/OrexinA-containing axons innervate locus coeruleus neurons that project to the Rat medial prefrontal cortex. Implication in the sleep-wakefulness cycle and cortical activation. *Synapse* **65**:843–857. doi:10.1002/syn.20912

España RA, Melchior JR, Roberts DCS, Jones SR. 2011. Hypocretin 1/orexin A in the ventral tegmental area enhances dopamine responses to cocaine and promotes cocaine self-administration. *Psychopharmacology* **214**:415–426. doi:10.1007/s00213-010-2048-8

España RA, Oleson EB, Locke JL, Brookshire BR, Roberts DCS, Jones SR. 2010. The hypocretin-orexin system regulates cocaine self-administration via actions on the mesolimbic dopamine system. *Eur J Neurosci* **31**:336–348. doi:10.1111/j.1460-9568.2009.07065.x

Evans A, Terstege DJ, Scott GA, Tsutsui M, Epp JR. 2022. Neurogenesis mediated plasticity is associated with reduced neuronal activity in CA1 during context fear memory retrieval. *Sci Rep* **12**:7016. doi:10.1038/s41598-022-10947-w

Fadel J, Burk JA. 2010. Orexin/hypocretin modulation of the basal forebrain cholinergic system: Role in attention. *Brain Res* **1314**:112–123. doi:10.1016/j.brainres.2009.08.046

Fadel J, Deutch AY. 2002. Anatomical substrates of orexin-dopamine interactions: lateral hypothalamic projections to the ventral tegmental area. *Neuroscience* **111**:379–387. doi:10.1016/s0306-4522(02)00017-9

Fadel J, Frederick-Duus D. 2008. Orexin/hypocretin modulation of the basal forebrain cholinergic system: insights from in vivo microdialysis studies. *Pharmacol Biochem Behav* **90**:156–162. doi:10.1016/j.pbb.2008.01.008

Giardino WJ, Eban-Rothschild A, Christoffel DJ, Li S-B, Malenka RC, de Lecea L. 2018. Parallel circuits from the bed nuclei of stria terminalis to the lateral hypothalamus drive opposing emotional states. *Nat Neurosci* **21**:1084–1095. doi:10.1038/s41593-018-0198-x

Grafe LA, Cornfeld A, Luz S, Valentino R, Bhatnagar S. 2017. Orexins Mediate Sex Differences in the Stress Response and in Cognitive Flexibility. *Biol Psychiatry* **81**:683–692. doi:10.1016/j.biopsych.2016.10.013

Grafe LA, Eacret D, Dobkin J, Bhatnagar S. 2018. Reduced Orexin System Function Contributes to Resilience to Repeated Social Stress. *eNeuro* **5**. doi:10.1523/ENEURO.0273-17.2018

Gunaydin LA, Grosenick L, Finkelstein JC, Kauvar IV, Fenno LE, Adhikari A, Lammel S, Mirzabekov JJ, Airan RD, Zalocusky KA, Tye KM, Anikeeva P, Malenka RC, Deisseroth K. 2014. Natural neural projection dynamics underlying social behavior. *Cell* **157**:1535–1551. doi:10.1016/j.cell.2014.05.017

Hara J, Beuckmann CT, Nambu T, Willie JT, Chemelli RM, Sinton CM, Sugiyama F, Yagami K, Goto K, Yanagisawa M, Sakurai T. 2001. Genetic ablation of orexin neurons in mice results in narcolepsy, hypophagia, and obesity. *Neuron* **30**:345–354. doi:10.1016/s0896-6273(01)00293-8

Hasegawa E, Maejima T, Yoshida T, Masseck OA, Herlitze S, Yoshioka M, Sakurai T, Mieda M. 2017. Serotonin neurons in the dorsal raphe mediate the anticataplectic action of orexin neurons by reducing amygdala activity. *Proc Natl Acad Sci U S A* **114**:E3526–E3535. doi:10.1073/pnas.1614552114

Hasegawa E, Yanagisawa M, Sakurai T, Mieda M. 2014. Orexin neurons suppress narcolepsy via 2 distinct efferent pathways. *J Clin Invest* **124**:604–616. doi:10.1172/JCI71017

Hashikawa K, Hashikawa Y, Falkner A, Lin D. 2016. The neural circuits of mating and fighting in male mice. *Curr Opin Neurobiol* **38**:27–37. doi:10.1016/j.conb.2016.01.006

Hashikawa K, Hashikawa Y, Tremblay R, Zhang J, Feng JE, Sabol A, Piper WT, Lee H, Rudy B, Lin D. 2017. Esr1+ cells in the ventromedial hypothalamus control female aggression. *Nat Neurosci* **20**:1580–1590. doi:10.1038/nn.4644

Hashikawa Y, Hashikawa K, Falkner AL, Lin D. 2017. Ventromedial Hypothalamus and the Generation of Aggression. *Front Syst Neurosci* **11**:94. doi:10.3389/fnsys.2017.00094

Hofer MA. 1996. Multiple regulators of ultrasonic vocalization in the infant rat. *Psychoneuroendocrinology* **21**:203–217. doi:10.1016/0306-4530(95)00042-9

Hong W, Kim D-W, Anderson DJ. 2014. Antagonistic control of social versus repetitive self-grooming behaviors by separable amygdala neuronal subsets. *Cell* **158**:1348–1361. doi:10.1016/j.cell.2014.07.049

Hull EM, Dominguez JM. 2007. Sexual behavior in male rodents. *Horm Behav* **52**:45–55. doi:10.1016/j.yhbeh.2007.03.030

Inutsuka A, Yamanaka A. 2013. The regulation of sleep and wakefulness by the hypothalamic neuropeptide orexin/hypocretin. *Nagoya J Med Sci* **75**:29–36.

Karnani MM, Schöne C, Bracey EF, González JA, Viskaitis P, Li H-T, Adamantidis A, Burdakov D. 2020. Role of spontaneous and sensory orexin network dynamics in rapid locomotion initiation. *Prog Neurobiol* **187**:101771. doi:10.1016/j.pneurobio.2020.101771

Kayaba Y, Nakamura A, Kasuya Y, Ohuchi T, Yanagisawa M, Komuro I, Fukuda Y, Kuwaki T. 2003. Attenuated defense response and low basal blood pressure in orexin knockout mice. *Am J Physiol Regul Integr Comp Physiol* **285**:R581-93. doi:10.1152/ajpregu.00671.2002

Keller M, Douhard Q, Baum MJ, Bakker J. 2006. Sexual experience does not compensate for the disruptive effects of zinc sulfate--lesioning of the main olfactory epithelium on sexual behavior in male mice. *Chem Senses* **31**:753–762. doi:10.1093/chemse/bjl018

Kingsbury L, Huang S, Wang J, Gu K, Golshani P, Wu YE, Hong W. 2019. Correlated Neural Activity and Encoding of Behavior across Brains of Socially Interacting Animals. *Cell* **178**:429-446.e16. doi:10.1016/j.cell.2019.05.022

Lauer J, Zhou M, Ye S, Menegas W, Nath T, Rahman MM, Di Santo V, Soberanes D, Feng G, Murthy VN, Lauder G, Dulac C, Mathis MW, Mathis A. 2021. Multi-animal pose estimation and tracking with DeepLabCut. *bioRxiv*. doi:10.1101/2021.04.30.442096

Lee W, Fu J, Bouwman N, Farago P, Curley JP. 2019. Temporal microstructure of dyadic social behavior during relationship formation in mice. *PLoS One* **14**:e0220596. doi:10.1371/journal.pone.0220596

Li Y, Zhong W, Wang D, Feng Q, Liu Z, Zhou J, Jia C, Hu F, Zeng J, Guo Q, Fu L, Luo M. 2016. Serotonin neurons in the dorsal raphe nucleus encode reward signals. *Nat Commun* **7**. doi:10.1038/ncomms10503

Lo L, Yao S, Kim D-W, Cetin A, Harris J, Zeng H, Anderson DJ, Weissbourd B. 2019. Connectional architecture of a mouse hypothalamic circuit node controlling social behavior. *Proc Natl Acad Sci U S A* **116**:7503–7512. doi:10.1073/pnas.1817503116

Lungwitz EA, Molosh A, Johnson PL, Harvey BP, Dirks RC, Dietrich A, Minick P, Shekhar A, Truitt WA. 2012. Orexin-A induces anxiety-like behavior through interactions with glutamatergic receptors in the bed nucleus of the stria terminalis of rats. *Physiol Behav* **107**:726–732. doi:10.1016/j.physbeh.2012.05.019

Marlin BJ, Mitre M, D'amour JA, Chao MV, Froemke RC. 2015. Oxytocin enables maternal behaviour by balancing cortical inhibition. doi:10.1038/nature14402

Meng C, Zhou J, Papaneri A, Peddada T, Xu K, Cui G. 2018. Spectrally Resolved Fiber Photometry for Multi-component Analysis of Brain Circuits. *Neuron* **98**:707-717.e4. doi:10.1016/j.neuron.2018.04.012

Mitchell CS, Fisher SD, Yeoh JW, Pearl AJ, Burton NJ, Bains JS, McNally GP, Andrews ZA, Graham BA, Dayas CV. 2020. A ventral striatal-orexin/hypocretin circuit modulates approach but not consumption of food. *bioRxiv*. doi:10.1101/2020.03.05.979468

Moda-Sava RN, Murdock MH, Parekh PK, Fetcho RN, Huang BS, Huynh TN, Witztum J, Shaver DC, Rosenthal DL, Alway EJ, Lopez K, Meng Y, Nellissen L, Grosenick L, Milner TA, Deisseroth K, Bito H, Kasai H, Liston C. 2019. Sustained rescue of prefrontal circuit dysfunction by antidepressant-induced spine formation. *Science* **364**. doi:10.1126/science.aat8078

Morse AM, Sanjeev K. 2018. Narcolepsy and Psychiatric Disorders: Comorbidities or Shared Pathophysiology? *Med Sci (Basel)* **6**. doi:10.3390/medsci6010016

Moy SS, Nadler JJ, Perez A, Barbaro RP, Johns JM, Magnuson TR, Piven J, Crawley JN. 2004. Sociability and preference for social novelty in five inbred strains: an approach to assess autistic-like behavior in mice. *Genes Brain Behav* **3**:287–302. doi:10.1111/j.1601-1848.2004.00076.x

Nilsson SRO, Goodwin NL, Choong JJ, Hwang S, Wright HR, Norville ZC, Tong X, Lin D, Bentzley BS, Eshel N, McLaughlin RJ, Golden SA. 2020. Simple Behavioral Analysis (SimBA) – an open source toolkit for computer classification of complex social behaviors in experimental animals. *bioRxiv*. doi:10.1101/2020.04.19.049452

Okuyama T. 2018. Social memory engram in the hippocampus. *Neurosci Res* **129**:17–23. doi:10.1016/j.neures.2017.05.007

Okuyama T, Kitamura T, Roy DS, Itohara S, Tonegawa S. 2016. Ventral CA1 neurons store social memory. *Science* **353**:1536–1541. doi:10.1126/science.aaf7003

Payet JM, Wilson K-E, Russo AM, Angiolino A, Kavanagh-Ryan W, Kent S, Lowry CA, Hale MW. 2021. Involvement of dorsal raphe nucleus serotonergic systems in social approach-avoidance behaviour and in the response to fluoxetine treatment in peri-adolescent female BALB/c mice. *Behav Brain Res* **408**:113268. doi:10.1016/j.bbr.2021.113268

Peyron C, Faraco J, Rogers W, Ripley B, Overeem S, Charnay Y, Nevsimalova S, Aldrich M, Reynolds D, Albin R, Li R, Hungs M, Pedrazzoli M, Padigaru M, Kucherlapati M, Fan J, Maki R, Lammers GJ, Bouras C, Kucherlapati R, Nishino S, Mignot E. 2000. A mutation

in a case of early onset narcolepsy and a generalized absence of hypocretin peptides in human narcoleptic brains. *Nat Med* **6**:991–997. doi:10.1038/79690

Quaedackers L, van Gilst MM, van Mierlo P, Lammers G-J, Dhondt K, Amesz P, Peeters E, Hendriks D, Vandenbussche N, Pillen S, Overeem S. 2019. Impaired social functioning in children with narcolepsy. *Sleep* **42**. doi:10.1093/sleep/zsy228

Rao RP, von Heimendahl M, Bahr V, Brecht M. 2019. Neuronal Responses to Conspecifics in the Ventral CA1. *Cell Rep* **27**:3460-3472.e3. doi:10.1016/j.celrep.2019.05.081

Reichenbach A, Clarke RE, Stark R, Lockie SH, Mequinion M, Dempsey H, Rawlinson S, Reed F, Sepehrizadeh T, DeVeer M, Munder AC, Nunez-Iglesias J, Spanswick DC, Mynatt R, Kravitz AV, Dayas CV, Brown R, Andrews ZB. 2022. Metabolic sensing in AgRP neurons integrates homeostatic state with dopamine signalling in the striatum. *Elife* **11**. doi:10.7554/eLife.72668

Sakurai T. 2005. Roles of orexin/hypocretin in regulation of sleep/wakefulness and energy homeostasis. *Sleep Med Rev* **9**:231–241. doi:10.1016/j.smrv.2004.07.007

Sakurai T, Amemiya A, Ishii M, Matsuzaki I, Chemelli RM, Tanaka H, Williams SC, Richardson JA, Kozlowski GP, Wilson S, Arch JR, Buckingham RE, Haynes AC, Carr SA, Annan RS, McNulty DE, Liu WS, Terrett JA, Elshourbagy NA, Bergsma DJ, Yanagisawa M. 1998. Orexins and orexin receptors: a family of hypothalamic neuropeptides and G protein-coupled receptors that regulate feeding behavior. *Cell* **92**:573–585. doi:10.1016/s0092-8674(00)80949-6

Samson WK, Taylor MM, Follwell M, Ferguson AV. 2002. Orexin actions in hypothalamic paraventricular nucleus: physiological consequences and cellular correlates. *Regul Pept* **104**:97–103. doi:10.1016/s0167-0115(01)00353-6

Saper CB, Lowell BB. 2014. The hypothalamus. *Curr Biol* **24**:R1111-6. doi:10.1016/j.cub.2014.10.023

Sargin D. 2019. The role of the orexin system in stress response. *Neuropharmacology* **154**:68–78. doi:10.1016/j.neuropharm.2018.09.034

Sasaki K, Suzuki M, Mieda M, Tsujino N, Roth B, Sakurai T. 2011. Pharmacogenetic modulation of orexin neurons alters sleep/wakefulness states in mice. *PLoS One* **6**:e20360. doi:10.1371/journal.pone.0020360

Silber MH, Krahn LE, Olson EJ, Pankratz VS. 2002. The epidemiology of narcolepsy in Olmsted County, Minnesota: a population-based study. *Sleep* **25(2)**:197-202. doi: 10.1093/sleep/25.2.197

Scott N, Prigge M, Yizhar O, Kimchi T. 2015. A sexually dimorphic hypothalamic circuit controls maternal care and oxytocin secretion. *Nature* **525**:519–522. doi:10.1038/nature15378

Soliman GA, Ishida-Takahashi R, Gong Y, Jones JC, Leshan RL, Saunders TL, Fingar DC, Myers MG Jr. 2007. A simple qPCR-based method to detect correct insertion of homologous targeting vectors in murine ES cells. *Transgenic Res* **16**:665–670. doi:10.1007/s11248-007-9110-2

Sterley T-L, Baimoukhametova D, Füzesi T, Zurek AA, Daviu N, Rasiah NP, Rosenegger D, Bains JS. 2018. Social transmission and buffering of synaptic changes after stress. *Nat Neurosci* **21**:393–403. doi:10.1038/s41593-017-0044-6

Takahashi A, Nagayasu K, Nishitani N, Kaneko S, Koide T. 2014. Control of intermale aggression by medial prefrontal cortex activation in the mouse. *PLoS One* **9**:e94657. doi:10.1371/journal.pone.0094657

Tsunematsu T, Kilduff TS, Boyden ES, Takahashi S, Tominaga M, Yamanaka A. 2011. Acute optogenetic silencing of orexin/hypocretin neurons induces slow-wave sleep in mice. *J Neurosci* **31**:10529–10539. doi:10.1523/JNEUROSCI.0784-11.2011

Tyree SM, Borniger JC, de Lecea L. 2018. Hypocretin as a Hub for Arousal and Motivation. *Front Neurol* **9**:413. doi:10.3389/fneur.2018.00413

Unger EK, Burke KJ Jr, Yang CF, Bender KJ, Fuller PM, Shah NM. 2015. Medial amygdalar aromatase neurons regulate aggression in both sexes. *Cell Rep* **10**:453–462. doi:10.1016/j.celrep.2014.12.040

van den Berg WE, Lamballais S, Kushner SA. 2015. Sex-specific mechanism of social hierarchy in mice. *Neuropsychopharmacology* **40**:1364–1372. doi:10.1038/npp.2014.319

Veening JG, Coolen LM. 2014. Neural mechanisms of sexual behavior in the male rat: emphasis on ejaculation-related circuits. *Pharmacol Biochem Behav* **121**:170–183. doi:10.1016/j.pbb.2013.12.017

Vittoz NM, Schmeichel B, Berridge CW. 2008. Hypocretin /orexin preferentially activates caudomedial ventral tegmental area dopamine neurons. *Eur J Neurosci* **28**:1629–1640. doi:10.1111/j.1460-9568.2008.06453.x

Wang Q-P, Koyama Y, Guan J-L, Takahashi K, Kayama Y, Shioda S. 2005. The orexinergic synaptic innervation of serotonin- and orexin 1-receptor-containing neurons in the dorsal raphe nucleus. *Regul Pept* **126**:35–42. doi:10.1016/j.regpep.2004.08.030

Wei D, Talwar V, Lin D. 2021. Neural circuits of social behaviors: Innate yet flexible. *Neuron* **109**:1600–1620. doi:10.1016/j.neuron.2021.02.012

Werling DM, Geschwind DH. 2013. Sex differences in autism spectrum disorders. *Curr Opin Neurol* **26**:146-153. doi: 10.1097/WCO.0b013e32835ee548.

Wu Z, Autry AE, Bergan JF, Watabe-Uchida M, Dulac CG. 2014. Galanin neurons in the medial preoptic area govern parental behaviour. *Nature* **509**:325–330. doi:10.1038/nature13307

Xie Y, Dorsky RI. 2017. Development of the hypothalamus: conservation, modification and innovation. *Development* **144**:1588–1599. doi:10.1242/dev.139055

Yang C, Zhang L, Hao H, Ran M, Li J, Dong H. 2019. Serotonergic neurons in the dorsal raphe nucleus mediate the arousal-promoting effect of orexin during isoflurane anesthesia in male rats. *Neuropeptides* **75**:25–33. doi:10.1016/j.npep.2019.03.004

Yang L, Zou B, Xiong X, Pascual C, Xie James, Malik A, Xie Julian, Sakurai T, Xie XS. 2013. Hypocretin/orexin neurons contribute to hippocampus-dependent social memory and synaptic plasticity in mice. *J Neurosci* **33**:5275–5284. doi:10.1523/JNEUROSCI.3200-12.2013

Yoshihara C, Numan M, Kuroda KO. 2018. Oxytocin and Parental Behaviors. *Curr Top Behav Neurosci* **35**:119–153. doi:10.1007/7854_2017_11

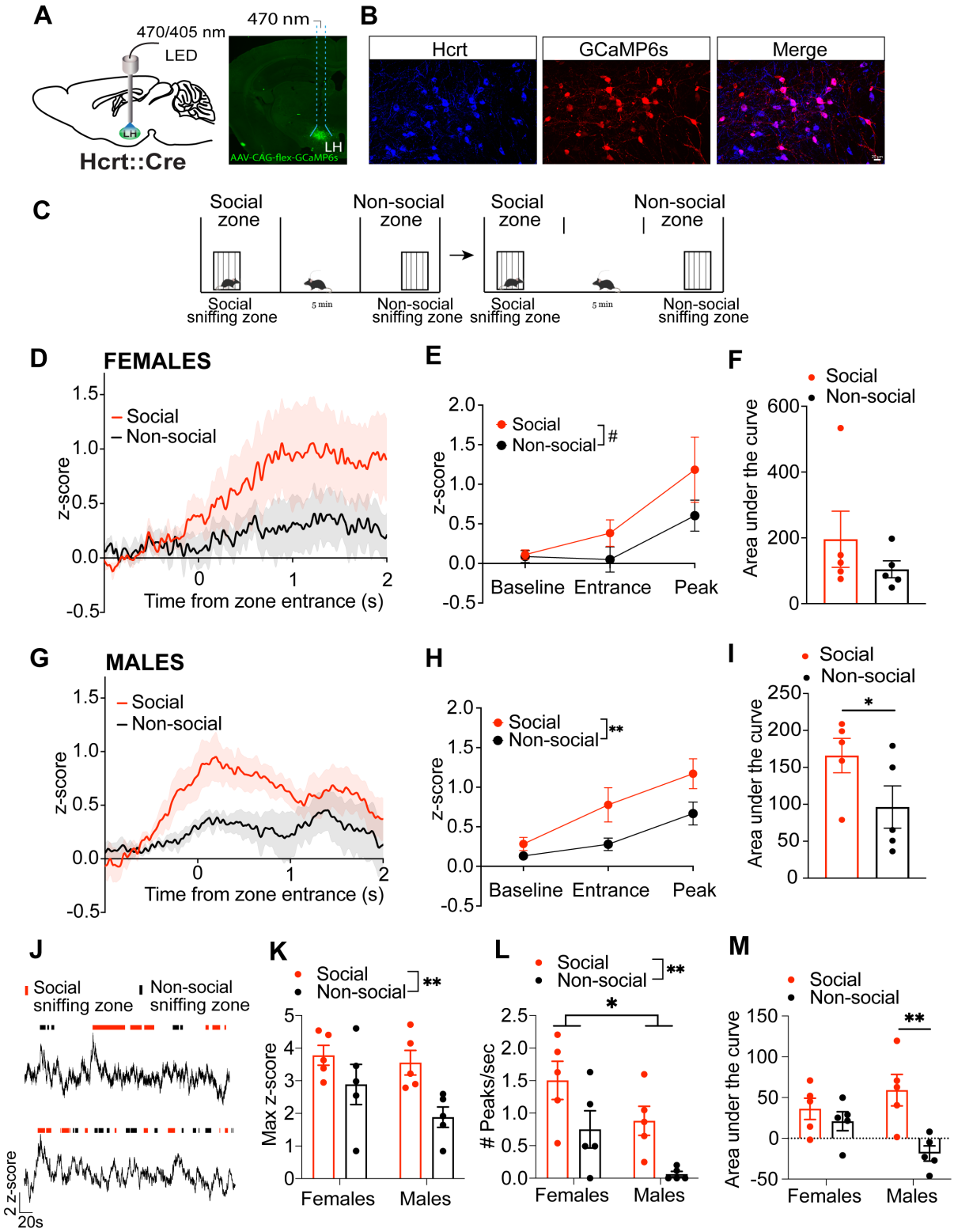

Figure 1. Increase in hcrt neuron activity in response to social investigation. A) Schematic (left) and a representative image (right) showing viral targeting and expression of GCaMP6s in LH hcrt neurons. **B)** Hypocretin-1 (blue) and GCaMP6s (red) co-localization in the LH of a *Hcrt*$^{IRES\text{-}Cre}$ mouse infused with the AAV-CAG-Flex-GCaMP6s. Scale bar, 20 um. **C)** 3-chamber social interaction paradigm during fiber photometry. Social and non-social zones are the compartments of the chamber that harbor the social target

or the empty cup, respectively. Sniffing zones are defined as the area around the perimeter of the holder zones. **D)** Averaged hcrt Ca^{2+} traces over time aligned to the time of entrance (t = 0 sec) into the social zone in female mice (n = 5 mice). **E)** The hcrt Ca^{2+} signal for each mouse showing baseline (-1 to 0 sec), entrance (0 sec) and peak response after the entrance into the social zone (0-2 sec). In female mice, the hcrt Ca^{2+} signal increased upon entrance into the social and non-social zones and the activity in each zone was comparable (two-way ANOVA; effect of time: $F(2, 24) = 8.15$, $p = 0.002$, effect of zone: $F(1, 24) = 3.25$, $^{\#}p = 0.084$). **F)** In female mice, the area under the curve of the averaged hcrt Ca^{2+} responses after entrance into social and non-social zones did not differ (paired t-test; $p = 0.39$). **G)** Averaged hcrt Ca^{2+} traces over time aligned to the time of entrance (t = 0 sec) into the social zone in male mice (n = 5 mice). **H)** In male mice, the hcrt Ca^{2+} signal increased upon entrance into the social and non-social zones and the activity in social zone was significantly greater than activity in the non-social zone (two-way ANOVA; effect of time: $F(2, 24) = 12.86$, $p = 0.0002$, effect of zone: $F(1,24) = 11.2$, $^{**}p = 0.0027$). **I)** In male mice, the area under the curve of the averaged hcrt Ca^{2+} responses after entrance into the social zone was significantly greater compared to the non-social zone (paired t-test; $^{*}p = 0.025$). **J)** A representative hcrt Ca^{2+} photometry trace aligned to the time spent in social (red) and non-social (black) sniffing zones from a female (above) and a male mouse (below). **K)** The maximum hcrt Ca^{2+} signal during interaction with the social target was larger compared with that during non-social target interaction in female and male mice (two-way ANOVA; effect of zone: $F(1, 16) = 9.23$, $^{**}p = 0.0078$, effect of sex: $F(1, 16) = 2.12$, $p = 0.16$). **L)** The frequency of activity (peaks/sec) during interaction with the social target was significantly larger compared to the non-social interaction. In females, the frequency of hcrt activity was larger during social and non-social interactions, compared with the male mice (two-way ANOVA; effect of zone: $F(1, 16) = 11.26$, $^{**}p = 0.004$, effect of sex: $F(1, 16) = 7.82$, $^{*}p = 0.013$). **M)** The area under the curve of the hcrt Ca^{2+} signal in each sniffing zone, normalized by the duration of time spent in each zone was significantly larger during interaction with the social target compared with the non-social target in male mice only (two-way ANOVA; zone X sex interaction: $F(1, 16) = 5.07$, $p = 0.039$; Tukey's multiple comparisons test: Social vs non-social sniffing zone; Males $^{**}p = 0.0055$, females $p = 0.86$). Data represent mean ± SEM.

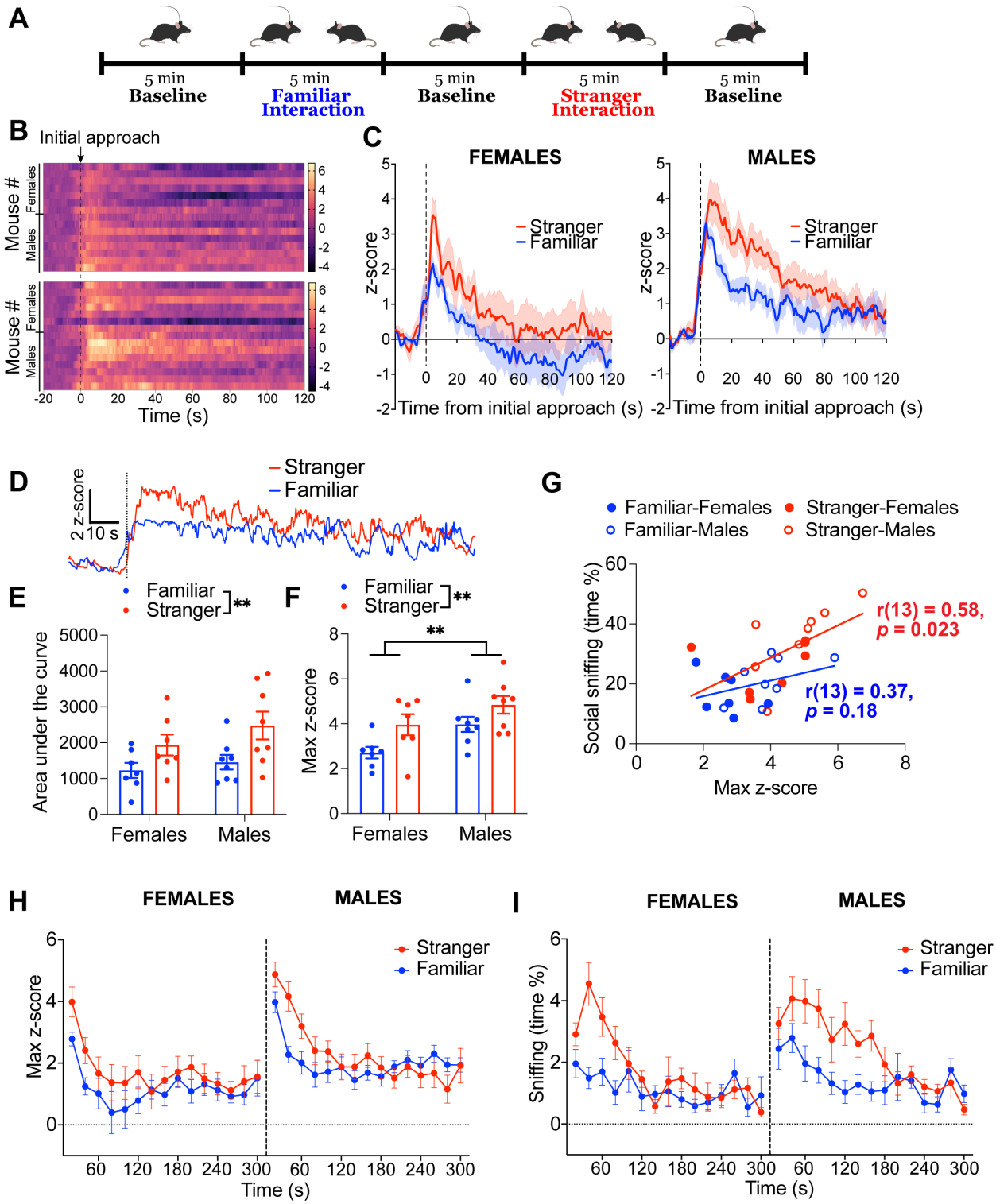

Figure 2. Differential hcrt neuron activity during social interaction in home cage. A) Experimental paradigm showing social interaction test during fiber photometry. After baseline recordings for 5 min in the home cage, the resident experimental mouse is introduced to a familiar (cage mate) followed by a stranger (novel) mouse. **B)** Heatmaps showing hcrt Ca^{2+} signal for each mouse 20 sec prior to and 2 min after being introduced to a familiar (top) or a stranger (bottom) mouse. Data are aligned to initial approach by the resident mouse. **C)** Averaged Ca^{2+} signal changes in hcrt

neurons in female (n = 7) and male (n = 8) mice during interaction with a stranger or a familiar mouse. The hcrt neuron activity peaks right after initial approach initiated by the experimental mouse and returns to baseline within 2 min. **D)** Representative hcrt Ca^{2+} traces from an experimental mouse during interaction with a stranger or a familiar mouse. **E)** The area under the curve of the hcrt Ca^{2+} response within the first 2 min of social behavior is larger when the resident mice interact with a stranger compared with a familiar mouse (two-way ANOVA; effect of conspecific: $F(1, 26) = 8.96$, $^{**}p = 0.006$, effect of sex: $F(1, 26) = 1.78$, $p = 0.19$). **F)** The maximum hcrt Ca^{2+} signal in response to initial approach and sniffing is larger when the resident mice are introduced to a stranger compared to a familiar cage mate. The hcrt Ca^{2+} signal is larger in male mice compared to female mice during interaction with familiar and stranger conspecifics (two-way ANOVA; effect of conspecific: $F(1, 26) = 8.01$, $^{**}p = 0.009$, effect of sex: $F(1, 26) = 8.29$, $^{**}p = 0.008$). **G)** Scatter plot showing the correlation between the maximum hcrt Ca^{2+} signal in the resident mice and the time they spent sniffing the stranger ($r(13)=0.58$, $^{*}p=0.023$) or the familiar ($r(13)=0.37$, $p=0.18$) conspecific. **(H)** The maximum hcrt Ca^{2+} signal in the resident mice over time during social behavior is shown for both females and males. The greater hcrt activity right after first approach and sniffing decreased over time in both females and males (three-way ANOVA; time X conspecific interaction: $F(14, 364) = 2.32$, $p = 0.004$; Tukey's multiple comparisons test: Stranger vs familiar at 20 sec $p = 0.035$, 40 sec $p = 0.009$, all other time points *p's* > 0.05). Male mice showed a greater hcrt Ca^{2+} signal within the first minute of social behavior, compared with females (three-way ANOVA; time X sex interaction: $F(14, 364) = 2.19$, $p = 0.007$; Tukey's multiple comparisons test: Male vs female at 20 sec $p = 0.013$, 40 sec $p = 0.033$, all other time points *p's* > 0.05). **I)** Time spent sniffing by the resident mice over time during social behavior is shown for females and males. Mice spent more time sniffing the stranger compared to familiar, which declined over time (three-way ANOVA; time X conspecific interaction: $F (14, 364) = 3.46$, $p < 0.001$, Tukey's multiple comparisons test: Stranger vs familiar at 40 sec $p < 0.001$, 60 sec $p = 0.0013$, 80 sec $p = 0.005$ all other time points *p's* > 0.05). Male mice engaged more in social interaction than females (three-way ANOVA; effect of sex: $F(1, 26) = 4.62$, $p = 0.041$). $^{*}p<0.05$, $^{**}p<0.01$. Data represent mean ± SEM. The complete statistical output is shown in Supplemental Table.

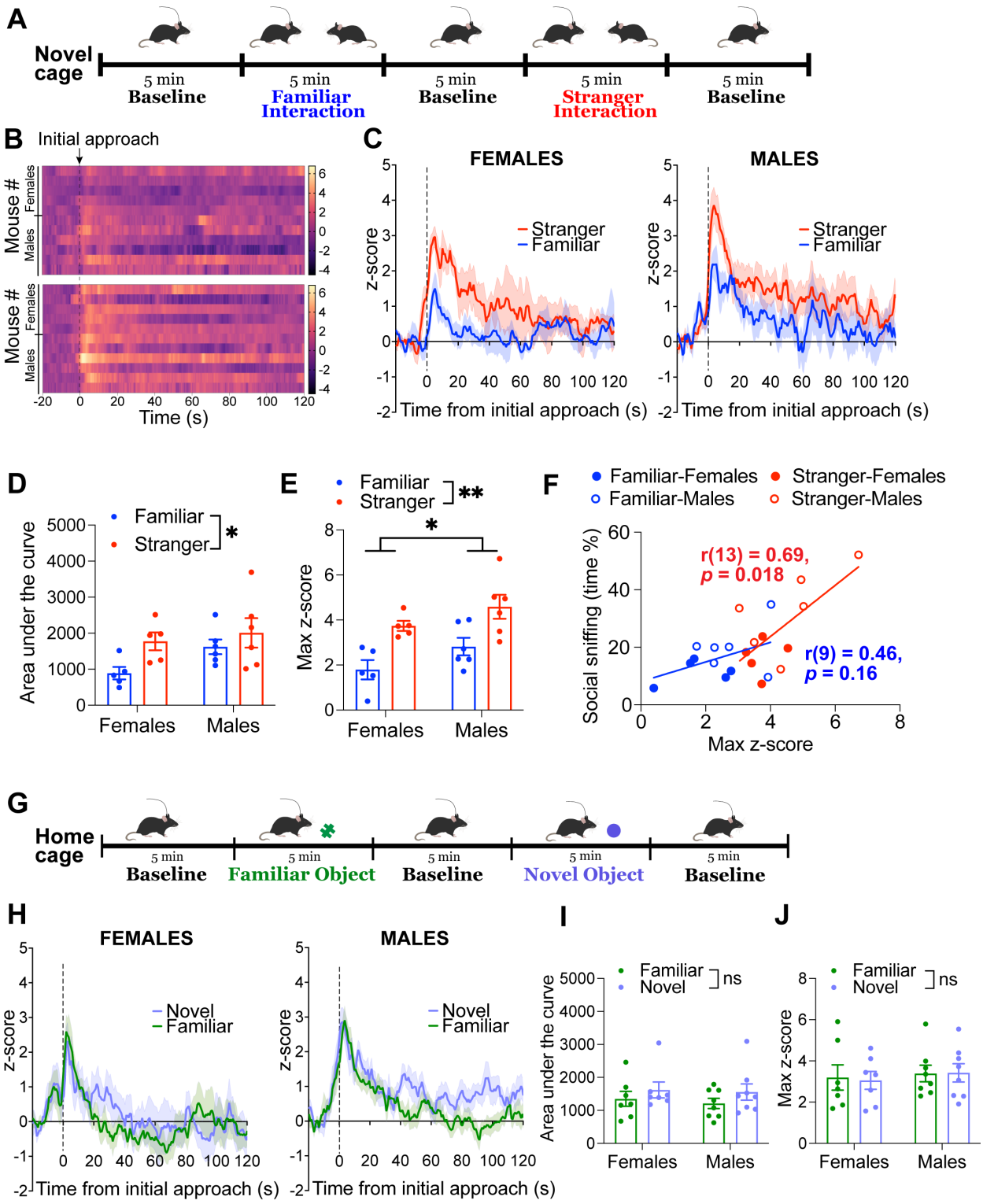

Figure 3. Differential hcrt activity during social interaction persists in a non-territorial setting and is absent during object investigation. A) Experimental paradigm showing social interaction in the novel cage test during fiber photometry. After baseline recordings for 5 min in a cage with novel bedding, the resident experimental mouse is introduced to a familiar (cage mate) followed by a stranger (novel) mouse. **B)** Heatmaps showing hcrt Ca^{2+} signal for each mouse 20 sec prior to and 2

min after being introduced to a familiar (top) or a stranger (bottom) mouse. Data are aligned to initial approach by the experimental mouse. **C)** Averaged Ca^{2+} signal changes in hcrt neurons in female (n = 5) and male (n = 6) mice during interaction with a stranger or a familiar mouse in the novel cage. The hcrt neuron activity peaks right after initial approach initiated by the experimental mouse and returns to baseline within 2 min. **D)** The area under the curve of the hcrt Ca^{2+} response within the first 2 min of social behavior is larger when the experimental mice interact with a stranger compared with a familiar mouse (two-way ANOVA; effect of conspecific: $F(1, 18) = 4.91$, $*p = 0.038$, effect of sex: $F(1, 18) = 2.83$, $p = 0.11$). **E)** The maximum hcrt Ca^{2+} signal in response to initial approach and sniffing is larger when the experimental mice are introduced to a stranger compared to a familiar cage mate. The hcrt Ca^{2+} signal is greater in male mice compared to female mice regardless of the social interaction type (two-way ANOVA; effect of conspecific: $F(1, 18) = 19.14$, $**p = 0.0004$, effect of sex: $F(1, 18) = 4.87$, $*p = 0.041$). **F)** Scatter plot showing the correlation between the maximum hcrt Ca^{2+} signal in the experimental mice and the time they spent sniffing the stranger $r(13)=0.69$, $*p=0.018$) or the familiar ($r(13)=0.46$, $p=0.16$) conspecific. **G)** Experimental paradigm showing fiber photometry during object interaction test. After baseline recordings for 5 min in the home cage, the resident experimental mouse is introduced to a familiar or a novel object. **H)** Averaged Ca^{2+} signal changes in hcrt neurons in female (n = 7) and male (n = 8) mice during interaction with a familiar or a novel object in the home cage, aligned to the time of initial approach to the object. **I)** The area under the curve of the hcrt Ca^{2+} response within the first 2 min of object interaction is comparable when the experimental mice interact with novel or familiar objects (two-way ANOVA; effect of object: $F(1, 26) = 1.97$, $p = 0.17$, effect of sex: $F(1, 26) = 0.21$, $p = 0.65$). **J)** The maximum hcrt Ca^{2+} signal in response to initial approach to familiar and novel objects is comparable (two-way ANOVA; effect of object: $F(1, 26) = 0.013$, $p = 0.91$, effect of sex: $F(1, 26) = 0.35$, $p = 0.56$). $*p<0.05$, $**p<0.01$, ns; non-significant. Data represent mean ± SEM.

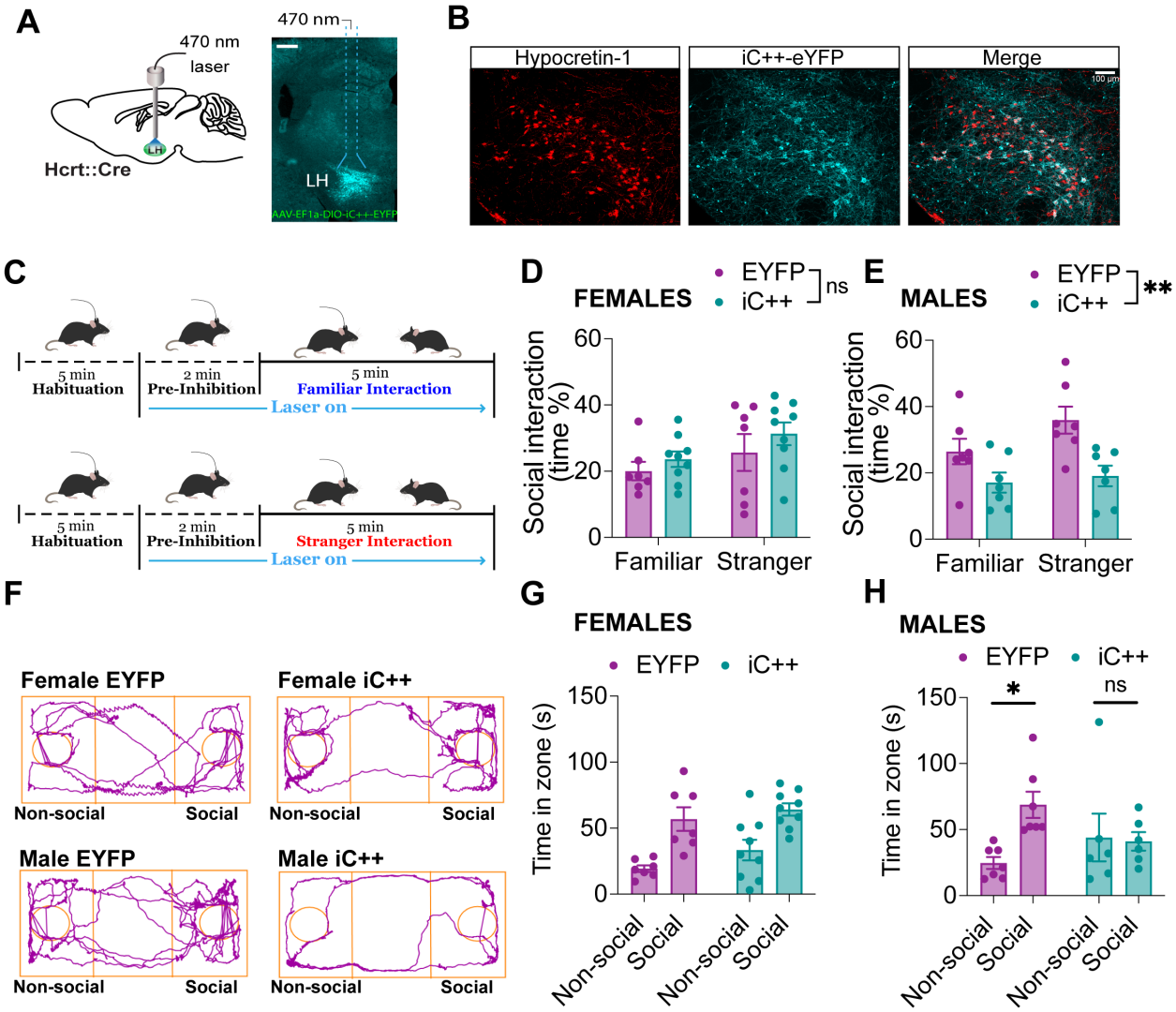

Figure 4. Acute optogenetic inhibition of hcrt neuron activity disrupts social interaction in male mice. A) Schematic (left) and a representative image showing viral targeting and expression of iC++ in LH hcrt neurons. **B)** Hypocretin-1 (red) and iC++ (cyan) co-localization in the LH of a *Hcrt*$^{IRES\text{-}Cre}$ mouse infused with the AAV-EF1a-DIO-iC++-EYFP. Scale bar, 100 um. **C)** Experimental paradigm showing 5 min social interaction with familiar or stranger mice after 5 min of fiber habituation and 2 min of hcrt neuron inhibition. Blue light was kept on during social interaction. Each interaction was performed on different days and the order of conspecific was counterbalanced. **D)** In female mice, optogenetic inhibition of hcrt neuron activity did not affect the time spent interacting with familiar or stranger conspecifics (two-way ANOVA; effect of group: $F(1, 28) = 1.64$, $p = 0.21$, effect of conspecific: $F(1, 28) = 3.41$, $p = 0.07$). **E)** Inhibition of hcrt neuron activity in male mice reduced interaction time with conspecifics, compared with EYFP mice (two-way ANOVA; effect of group: $F(1, 24) = 13.82$, $^{**}p = 0.001$, effect of conspecific: $F(1, 24) = 2.66$, $p = 0.12$) **F)** Representative tracks from female and male EYFP and iC++ mice during in 3-chamber sociability task in the presence of blue light. **G)** Inhibition of hcrt neuron activity did not lead to a change in sociability in females in 3-chamber test (two-way ANOVA; effect of group: $F(1, 28) = 2.59$, $p = 0.12$, effect of zone: $F(1, 28) = 26.56$, $p < 0.001$). **H)** Male iC++ mice spent comparable time in the social and non-social sniffing zones of the 3-chamber in contrast to male EYFP mice (two-way ANOVA; group X zone interaction: $F(1, 22) = 4.81$, $^{*}p = 0.039$; Tukey's multiple comparisons test: EYFP social vs non-social $p = 0.029$, iC++ social vs non-social $p = 0.99$). Data represent mean ± SEM.